Journal of Hazardous Materials 323 (2017) 471–477

Contents lists available at ScienceDirect

Journal of Hazardous Materials

journal homepage: www.elsevier.com/locate/jhazmat

Assessment of the abatement of acelsulfame K using cerium doped ZnO as photocatalyst

P. Calza [a], C. Gionco [a], M. Giletta [a], M. Kalaboka [b], V.A. Sakkas [b], T. Albanis [b], M.C. Paganini [a,*]

[a] Department of Chemistry, Via Giuria 7, 10125 Torino, Italy
[b] Department of Chemistry, Laboratory of Analytical Chemistry, Ioannnina 45 110, Greece

HIGHLIGHTS

- Hydrothermal synthesis and characterization of Ce doped ZnO.
- The abatement of ACE K is assessed in ultrapure water and in river water matrix.
- Demonstrated higher degradation activity than P25 under visible light.
- The degradation activity is less affected in river water than for P25.

GRAPHICAL ABSTRACT

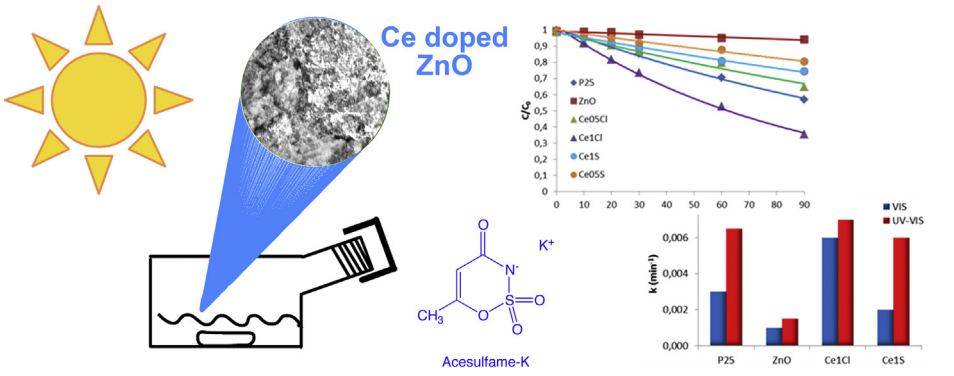

ARTICLE INFO

Article history:
Received 29 December 2015
Received in revised form 30 March 2016
Accepted 31 March 2016
Available online 2 April 2016

Keywords:
Acesulfame K
Cerium
Zinc oxide
River water

ABSTRACT

In the present study, we investigated the possibility to abate Acesulfame K, a persistent emerging contaminant, in aqueous media using zinc oxide based materials. For this purpose, bare and Ce-doped zinc oxide was prepared via an easy and cheap hydrothermal process using different cerium salts as precursors. Their photocatalytic performance was evaluated in different media, namely ultrapure and river water under both UV–vis and visible light. Commercial TiO_2 P25 was also employed and used as a reference photocatalyst for comparison purposes. The obtained results pointed out that cerium doped zinc oxide composites exhibit higher performance than TiO_2 P25, especially under visible light and in the presence of organic matter, when the activity of the latter is greatly depressed. In particular, ZnO doped with cerium (1%) was the most effective material, and could be a promising alternative to TiO_2 P25, especially in the treatment of natural waters.

1. Introduction

Artificial sweeteners are often used as a substitute for sucrose in a considerable variety of foods and beverages [1]; as an example, the global consumption of acesulfame (ACE), saccharin (SAC) and cyclamate (CYC) in the United States was estimated to be 5, 37 and 47 kt/year, respectively [2]. They are used in other personal

* Corresponding author.
E-mail address: mariacristina.paganini@unito.it (M.C. Paganini).

http://dx.doi.org/10.1016/j.jhazmat.2016.03.093
0304-3894/

care and pharmaceutical products, such as toothpastes, as well [3]. Their remarkable chemical stability causes a scarce elimination in conventional treatment systems and their subsequent release into water bodies, as assessed by recent studies [4]; as such, artificial sweeteners have been detected at ppt level in several rivers and lakes in European countries and North America [5]. In particular, acesulfame and sucralose are recognized as the most persistent [6] and, for this reason, they were valued as ideal markers for pollution in surface water and groundwater [7]. Recently, Gan et al. estimated for acesulfame half-lives ranging from 4 to 112 days [8] in water under environmentally relevant conditions (including direct and indirect photolysis, biodegradation and hydrolysis). These findings significantly highlight another critical issue: namely, the formation and accumulation of potentially more deleterious by-products from natural degradation [1]. Hence, there is a need to develop effective purification methods for eliminating those emerging organic contaminants (EOCs) from water. In this sense, advanced oxidation processes (AOPs) and in particular heterogeneous photocatalys could be highly promising [9].

Semiconductors oxides such as TiO_2, ZnO, WO_3 etc, have been attempted for the photocatalytic degradation of a wide variety of environmental contaminants [10–12]. Even if TiO_2 is usually considered the most photoactive catalyst [13], ZnO could be a suitable alternative thanks to its very similar band gap and the huge number of different morphologies in which it can be prepared [14]. In particular, doped zinc oxide is a promising candidate when using solar light, as assessed by the high photoactivity showed by Cu-doped ZnO in the degradation of organic pollutants [15]. Recently, doping with lanthanides got a lot of interest; a recent study on zirconium oxide doped with cerium demonstrated good properties in charge separation with visible light, despite the huge band gap of zirconia, thanks to the singular electronic properties of cerium [16].

In this framework, we synthetized different photocatalysts based on ZnO doped with a very low amount of cerium, aimed to develop new materials capable to use solar light for the abatement of organic persistent pollutants of emerging concern. More specifically, pure and doped ZnO with low cerium loading (0.5 and 1% M) were synthesized via hydrothermal process, a simple and green process to obtain controlled nanostructures at low temperatures. This way of synthesis, in comparison to other techniques is fast cheap and highly efficient. The precursor used are easily reachable and the amount of rare earth compound employed is so low that do not affect the final price of the catalyst. The morphological and textural characteristics, the crystal structure and optical properties of the synthesized materials were investigated and their photocatalytic efficiency was assessed towards the abatement of acesulfame K (ACE) under solar light and visible light in different aqueous matrices.

2. Experimental

2.1. Samples preparation

All reactants employed in this work were purchased from Sigma-Aldrich (Milan Italy) and used without any further purification treatment. Bare ZnO sample was synthesized starting from a water solution of zinc acetate. Then a 4 M NaOH solution was added dropwise until the pH was 10–11. Finally the solution was transferred into a Teflon lined stainless steel 100 mL autoclave (filling 70%), and treated at 175 °C overnight. The product was centrifuged at 6000 rpm and dried at 70 °C overnight.

The Ce doped ZnO sample (Ce molar concentration 0.5 and 1%) was prepared adding, in the starting solution, two different precursors salts in stoichiometric amount: $CeCl_3{\cdot}7H_2O$ and $Ce(SO_4)_2$, respectively. Hereafter the doped samples will be labelled as Ce05Cl and Ce1Cl for what concerns the samples doped with cerium chloride and Ce05S and Ce1S for the samples with cerium sulphate.

2.2. Characterization techniques

X-rays powder diffraction (XRPD) patterns were recorded using a PANalytical PW3040/60 X'Pert PRO MPD Lissone (MI) Italy (45 kV, 40 mA) with a copper Kα radiation source (0.15418 nm). Samples were scanned continuously in the 2θ range between 10° and 100° (step size 0.0167°, time per step 20 s). The X'Pert High-Score software was used to identify the mineral phases present in the samples.

Rietveld refinement was performed on the diffraction patterns to determine the crystallite size and relative abundance of phases (on the basis of the intensity of reflections, the density, and the mass absorption coefficient of the identified mineral phases), using the MAUD 2.26 software and a NIST Si powder to determine the instrumental broadening [17].

The morphology of the materials was studied by scanning electron microscopy (SEM) using a JOEL microscope (JSM-6510-LV, JEOL, Tokyo, Japan) equipped with Energy Dispersive Spectroscopy Analyzer (EDS x-act, Oxford Instrument).

The UV–vis absorption spectra were recorded using a Varian Cary 5000 spectrophotometer, coupled with an integration sphere for diffuse reflectance studies (DRS), using a Carywin-UV/scan software. A sample of PTFE with 100% reflectance was used as reference.

The surface area measurements were carried out on a Micromeritics Accelerated Surface Area and Porosimetry System (ASAP) 2020/2010 using the Brunauer–Emmett–Teller (B.E.T.) equation on the N_2 adsorption measurement. Prior to the adsorption run, all the samples were outgassed at 160 °C for 3 h.

A PHI 5000 Versaprobe II Scanning X-ray Photoelectron Spectrometer (monochromatic Al K-alpha X-ray source with 1486.6 eV energy) was used to investigate the surface chemical composition, with a focused 100 μm beam. The high resolution (HR) and survey spectra were recorded using a pass energy value of 23.5 eV and 187.85 eV respectively.

2.3. Irradiation procedure

The photocatalytic performance of the catalysts was assessed through the photocatalytic degradation of acelsulfame K (initial concentration, 20 mg L^{-1}) in a variety of experimental conditions, such as, different aqueous matrices (distilled and river water) at natural pH under simulated solar light as well as visible light. The catalysts (5 mg) were suspended in an aqueous solution of the sweetener in a 50 mL cylindrical quartz glass reactor that was positioned at 18 cm distance from light source under continuous stirring. Catalyst loadings were relatively low (100 mg L^{-1}) in order to obtain slower kinetics and compare the performance of the respectively materials, as well as to avoid dark zones in the illuminated slurry. Irradiation was carried out using a Suntest CPS+ apparatus from Heraeus (Hanau, Germany) equipped with a Xenon arc lamp (1500 W) and glass filters restricting the transmission of wavelengths below 290 nm (simulated solar light). An average irradiation intensity of 750 W m^{-2} was maintained throughout the experiments and was measured by internal radiometer. The corresponding light dose for 10 min of irradiation was 450 KJ m^{-2}. For visible light experiments a cut-off long pass filter was used (λ > 430 nm). Chamber temperature was regulated by pressurized air cooling circuit and monitored using thermocouples supplied by the manufacturer. The temperature of samples did not exceed 20 °C using tap water cooling circuit for the reactor. Before irradiation, the suspensions were allowed to stay in the dark for 60 min under stirring, to reach adsorption equilibrium on the surface of the catalysts. In all cases, to remove catalyst particles the solution samples were

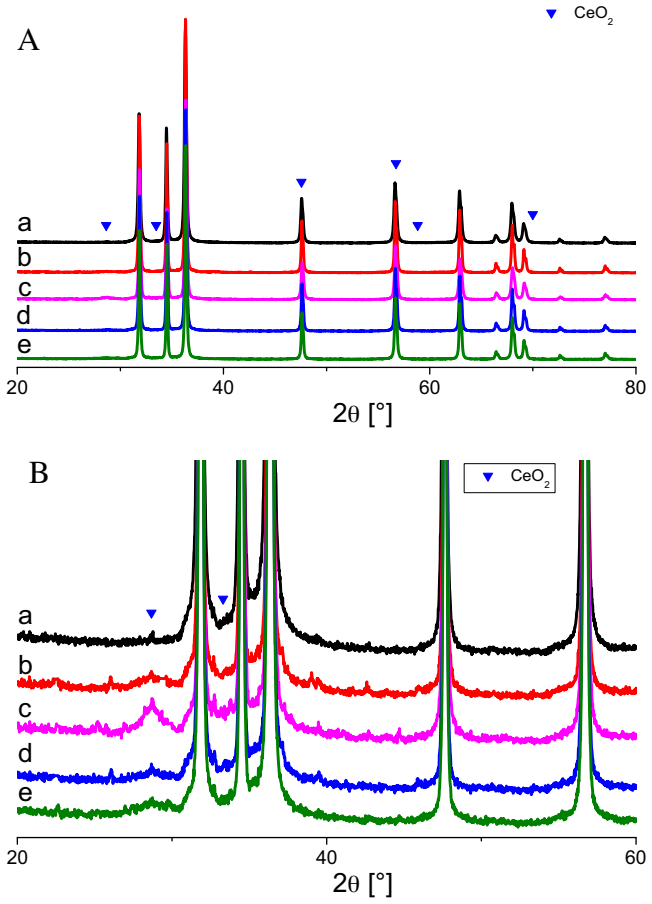

Fig. 1. XRPD patterns of (a) ZnO, (b) Ce05Cl, (c) Ce1Cl, (d) Ce05S and (e) Ce1S. Panel B is a magnification of panel A.

passed through 0.45 μm filters and were further analyzed with the appropriate analytical technique. Direct photolysis in the absence of catalyst was also performed as blank experiment in order to calculate its contribution in the degradation of the contaminant.

2.4. Samples analysis

The analysis was carried out using liquid chromatography (Dionex Ultimate 3000), equipped with an auto sampler and a UV-DAD detector. The analytical column was a Thermo Scientific Hypersil GOLD C18 column, (250 × 4.6 mm, 5 μm). A binary solvent system made of ACN and phosphate buffer (KH_2PO_4 0.0125 M, pH = 3.5) was used at 1.5 mL/min as follows: initial condition 8% ACN, then a linear ramp to 10% of ACN in 7 min; another ramp to 50% ACN in 5 min, (held for 3 min), and finally a linear ramp to 80% ACN in 1 min (held for 6 min). The column temperature was set at 30 °C. Detection was performed at 214 and 220 nm, whereas the characteristic UV absorption spectrum was used to confirm the identity of the chromatographic signals.

3. Results and discussion

3.1. Materials characterization

3.1.1. XRPD analysis

XRPD patterns of the samples investigated in this work are shown in Fig. 1. The pattern of undoped ZnO corresponding to (1 0 0), (0 0 2), (1 0 1), (1 0 2), (1 1 0), (1 0 3), (2 0 0), (1 1 2) and (2 0 1) planes are in accordance with the wurtzite hexagonal phase of ZnO [18]. The introduction of Ce does not bring relevant modifications in the crystal structure of ZnO; indeed, it segregates as CeO_2 phase even at a very low concentration of dopants, as it can be seen in Fig. 1B.

Table 1
Cell parameters and crystallite size obtained from Rietveld refinement of the XRPD patterns of bare and doped ZnO. R_{wp} is the weighted residual error, *a* and *c* are lattice parameters, d is the average crystallite dimension.

Sample	R_{wp}	a [Å]	c [Å]	d [nm]
ZnO	8.99	3.2520	5.2098	121
Ce05Cl	14.70	3.2528	5.2112	285
Ce1Cl	18.66	3.2469	5.2034	230
Ce05S	10.02	3.2538	5.2130	233
Ce1S	8.82	3.2524	5.2105	204

On the XRPD patterns a Rietveld refinement was performed using the MAUD software. Table 1 lists the calculated lattice parameters and average crystallites size. The lattice parameters of ZnO are not strongly influenced by the introduction of Ce. The ZnO crystallites are large, indeed the diffraction peaks are sharp and intense, and their size increases when Ce is added. On the other hand the CeO_2 crystallites obtained are significantly smaller, as evidenced by the broad and low intensity of its diffraction peaks. Because of the small amount and average size of the cerium oxide the results regarding this phase are not reported in Table 1 since they would not be fully reliable as a pair distribution function analysis would be needed for this kind of nanocrystals. This is also the reason for the higher R_{wp} (the weighted residual error) values of the refinement of the doped samples compared to the bare oxide.

3.1.2. Scanning electron microscopy

Fig. 2 depicts the surface morphology of pure ZnO and Ce-doped ZnO catalysts. The surface shows many inhomogeneous zones, however the majority of crystals look like quite large and most of them are formed by aggregates. To be more specific, the undoped ZnO (Fig. 2a) exhibited clusters of particles, with ZnO getting stacked on each other to give a look of a rough surface.

On the other hand, the doped catalysts (Fig. 2b and c) synthesized using cerium chloride and cerium sulphate, respectively, revealed flakes of particles with aggregates. In some cases, especially in the case of Ce1S, the surface shows the presence of spherical microstructures. Agglomeration of crystallites takes place leading to a cluster of a nearly spherical structure. Based on these observations it is concluded that cerium doping changes the morphology, and in particular the aggregation, of the final product.

The chemical compositional analysis is very important to monitor the concentration of the dopant. The EDS analysis of the described samples shows that, as expected, only Zn and O are present in the non-doped sample of ZnO and that the total percentage of cerium in the doped samples is about 0.45%. The Ce/Zn molar ratio calculated from the atomic percentages is close to 1%, as expected from the nominal composition.

3.1.3. X-ray photoelectron spectroscopy

The Ce1Cl and Ce1S samples were analyzed with the XPS technique in order to investigate the surface Ce^{3+}/Ce^{4+} ratio. The survey spectra (not shown) indicate the presence of Zn, O and Ce, with a small residue of chlorine for the Ce1Cl sample. In Table 2 the calculated (Ce/Zn) XPS atomic ratios, obtained from the integrated area of the spectra are also reported. The Ce1S sample has a Ce/Zn ratio of 0.8%, quite close with the nominal value of 1% and consistent with the results obtained with the EDS analysis. On the contrary, the Ce1Cl sample has a Ce/Zn ratio of 2%, which is twice from the expected nominal value and from the results obtained from the EDS (bulk) analysis. This is attributed to the fact that in the Ce1Cl sample the Ce atoms are not homogenously distributed, and that there

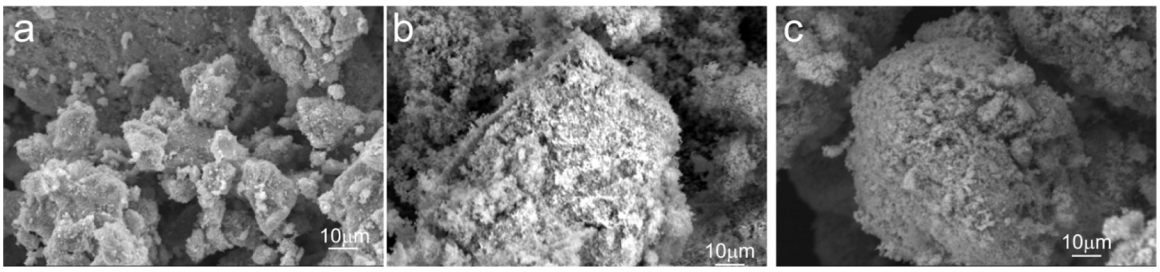

Fig. 2. SEM images of (a) ZnO, (b) Ce1Cl, (c) Ce1S.

Table 2
Atomic percentage of elements obtained from EDS and XPS analysis (see paragraph 3.1.5 for the details).

	EDS		XPS	
Sample	Elements	Atomic %	Ce/Zn ratio	Ce/Zn ratio
ZnO	O	38.79	/	
	Zn	61.21		
Ce1Cl	O	51.29	0.9%	2.2%
	Zn	48.26		
	Ce	0.45		
Ce1S	O	55.89	1.0%	0.8%
	Zn	44.11		
	Ce	0.44		

Table 3
Calculated energy gap (through the Tauc plot from DRS measures) and B.E.T. specific surface area (from nitrogen adsorption/desorption measures) of the samples.

Sample	E_g [eV]	S_{BET} [$m^2\ g^{-1}$]
TiO_2 P25	3.28	55 ± 3
ZnO	3.26	≤ 10
Ce–ZnO	3.27	≤ 10

is a concentration gradient between the bulk and the surface of the sample.

Fig. 4 depicts the high resolution XPS spectra in the Ce3d region and their deconvolution into the components corresponding to the various Ce transitions [19], the major components related to the presence of Ce^{3+} are also evidenced. The spectra are quite similar, nevertheless the features related to the presence of Ce^{3+} are more intense in the Ce1Cl sample. From the deconvolution it is possible to calculate the Ce^{3+}/Ce^{4+} ratio [20], according to the formula:

$$C_{Ce(III)} = \frac{v_0 + v' + u_0 + u'}{\Sigma_i(v^i + u^i)} \quad (1)$$

We obtained a value of 35% for Ce1Cl and of 29% for Ce1S. Despite the values are quite similar, this is a clear indication of a higher presence of Ce(III) in the sample prepared starting from the cerium(III) chloride salt.

3.1.4. DRS UV–vis analysis

Fig. 3 shows the absorption spectra obtained for ZnO and Ce doped ZnO samples. As it can be seen the Ce doped ZnO composites (Fig. 3c and d) display a very small modification in the overall absorption towards the visible domain (red shift), where a small shoulder is observed (Fig. 3 enlargement). The spectra are dominated by the valence band (VB)—conduction band (CB) transition occurring at about 400 nm for all the samples containing ZnO (bare and Ce doped), and at about 350 nm for TiO_2 P25 and it confirms previous data reported in the literature [21].

Energy gap values have been calculated (Table 3) by linearization of the plot reporting $(\alpha h\nu)^{1/2}$ vs $h\nu$ typical of indirect band gap transitions for TiO_2 P25 and by linearization of the plot reporting

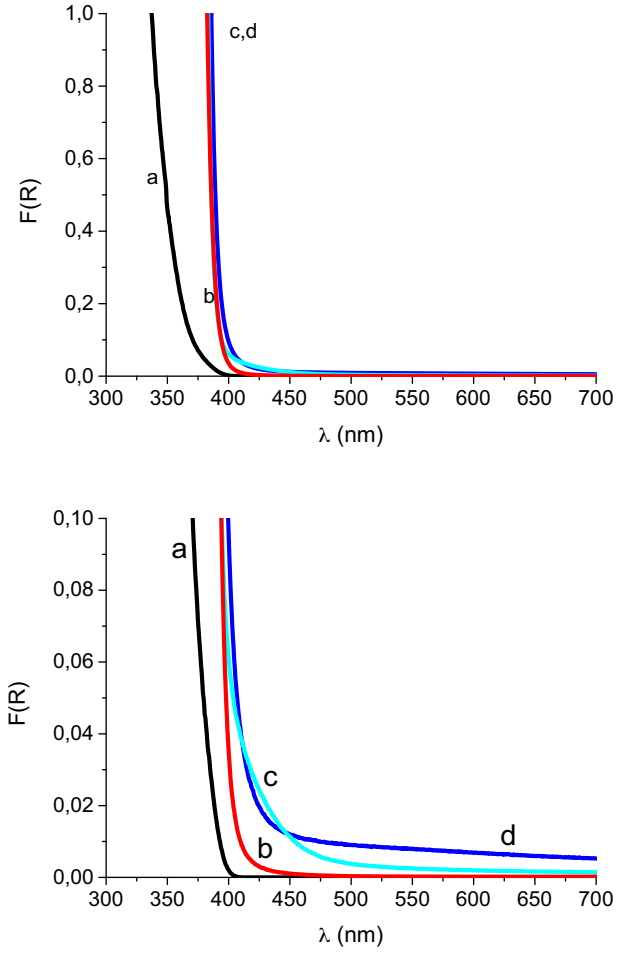

Fig. 3. Absorption spectra of TiO_2 P25 (a), ZnO (b), Ce1Cl (c) and Ce1S (d).

$(\alpha h\nu)^2$ vs $h\nu$ typical of direct band gap transitions for ZnO and Ce doped ZnO.

The calculated energy gaps for the three samples are very similar; the samples ZnO and Ce–ZnO show a band gap of 3.26 and 3.27 eV, respectively, whereas the P25 presents a band gap of 3.28 eV.

3.1.5. B.E.T. specific surface area

The specific surface area of the samples was measured applying the Brunauer–Emmett–Teller (B.E.T.) equation on the N_2 adsorption measurement. The S_{BET} of the ZnO and Ce doped ZnO samples (Table 3) was calculated at around 10 $m^2\ g^{-1}$, or even less, much lower compared to that of TiO_2 P25. This is quite in agreement with the large crystallite size found by the XRPD analysis.

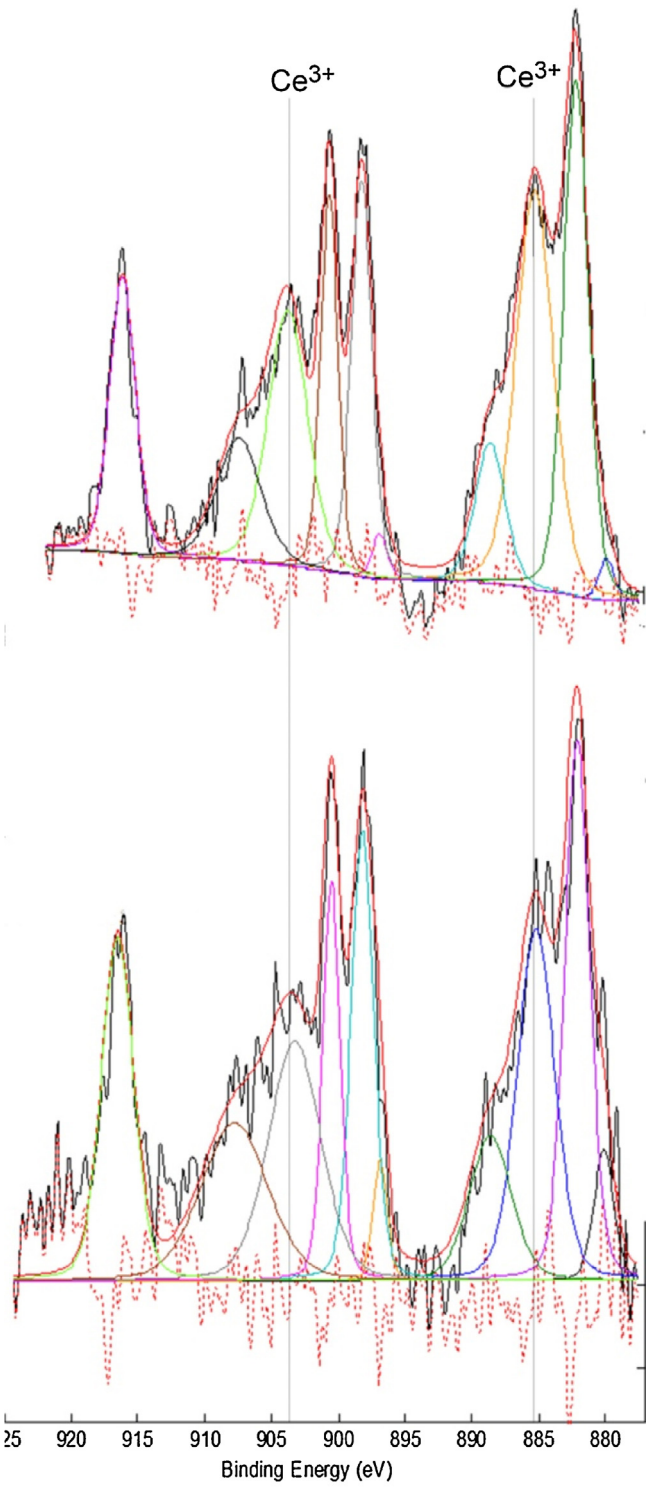

Fig. 4. XPS deconvoluted spectra of the Ce 3d region for the Ce1Cl (a) and Ce1S (b) samples.

3.2. Photocatalytic degradation of acesulfame K

The photocatalytic activity of ZnO based materials, as well as, TiO_2 P25, was evaluated under UV–vis and vis light in ultrapure water and in river water at natural pH, using ACE as a target molecule. The degradation curves for ACE as a function of irradiation time in ultrapure water are plotted in Fig. 5, while those in river water are shown in Fig. 6 (for comparison purpose, the profiles obtained with commercial TiO_2 P25 are depicted as well). The experiments revealed that the photocatalytic degradation of ACE can be ascribed to a pseudo-first order kinetic model, so that the disappearance initial rate can be calculated by using monoexponential decay, as described by the following equation:

$$C = C_0 e^{-kt} \quad (2)$$

where C corresponds to the pollutant concentration, k is the pseudo-first order kinetic constant, t is the reaction time and C_0 is pollutant concentration for t = 0. The calculated rate constants (k) in all experiments are reported in Fig. 7.

Results show that doped ZnO samples are more active than bare ZnO and TiO_2 P25 in ACE degradation, above all when using vis light only. However, irrespective of the light source, ACE degradation increases when increasing the dopant yield and is maxima with 1% of dopant. Some differences also arose when changing the dopant salt (namely $CeCl_3$, labelled Ce1Cl and Ce05Cl) and a Ce(IV) salt (namely $Ce(SO_4)_2$ labelled Ce1S and Ce05S). Results underlined that the materials doped with $CeCl_3$ salt are more active than those prepared starting from $Ce(SO_4)_2$, so implying a key role played by the cerium initial oxidation state. In particular, the best photocatalytic performance is obtained with ZnO doped with 1% $CeCl_3$ (named Ce1Cl).

Data obtained in ultrapure water show that the efficiency of TiO_2 P25 and ZnO decreased when passing from solar light (Fig. 5, panel A) to vis light (Fig. 5, panel B), while ZnO–Ce composites maintain a similar activity. In particular, for TiO_2 P25, the calculated rate constant k declines from 13×10^{-3} (simulated solar irradiation) to 6×10^{-3} min^{-1} (vis light), while for Ce1Cl k passes from 13×10^{-3} (simulated solar irradiation) to 11×10^{-3} min^{-1} (vis light, see Fig. 7). Therefore, it is important to notice that under Vis light ACE degradation with Ce1Cl becomes higher than TiO_2 P25, as k_{Ce1Cl3}/k_{P25} ratio passes from 1 (UV–vis) to 2 (vis).

The same experiments were performed in river water, with a dissolved organic matter content of 4.8 mg L^{-1}, employing bare materials and 1% doped materials. ACE photocatalytic degradation curves are plotted in Fig. 6.

Compared to ultrapure water, as expected ACE degradation followed slower kinetics. When employing P25, k declines from 13×10^{-3} to 6.5×10^{-3} min^{-1} in UV–vis and from 6×10^{-3} to 3×10^{-3} min^{-1} in vis light. Conversely, rate constant for doped ZnO Ce1Cl diminishes from 13×10^{-3} to 7×10^{-3} min^{-1} in UV–vis and from 11×10^{-3} to 6×10^{-3} min^{-1} in vis light. By analyzing the calculated rate constants ratio, again k_{Ce1Cl3}/k_{P25} ratio passes from 1 (under UV–vis) to 2 (vis only), so underlining that also in natural waters doped material still maintains a higher photocatalytic efficiency.

The overall data could be explained by taking into account several aspects. The increased photocatalytic effect observed in visible light could be attributed to the tiny shoulder evidenced in the absorption spectra of doped samples (see Fig. 3 enlargement) indicating the presence of intra-band gap states and not a real red-shift of the band gap itself [14,15]. We propose that these intra-band gap states are the responsible for the photocatalytic activity of the doped samples, allowing the absorption of visible photons through a step-by-step mechanism (vide infra). The greater efficiency of doped materials may be also linked to the complex electronic structure of cerium oxide. The ceria or cerium oxide(IV) has a band gap equal to 6 eV. However, the ceria has a special feature: the HOMO-LUMO transition occurs between the oxygen 2p orbitals (valence band) and 4f orbitals of the Ce ion, which are empty in the case of Ce^{4+} or partially filled in the case of Ce^{3+}. This peculiarity permits to increase possible transitions for electrons.

Doping zinc oxide with ceria allows to create materials that preserve the structure of ZnO, but in which some interaction at the interfaces of the two oxides occurs. Indeed, even if the two oxides do

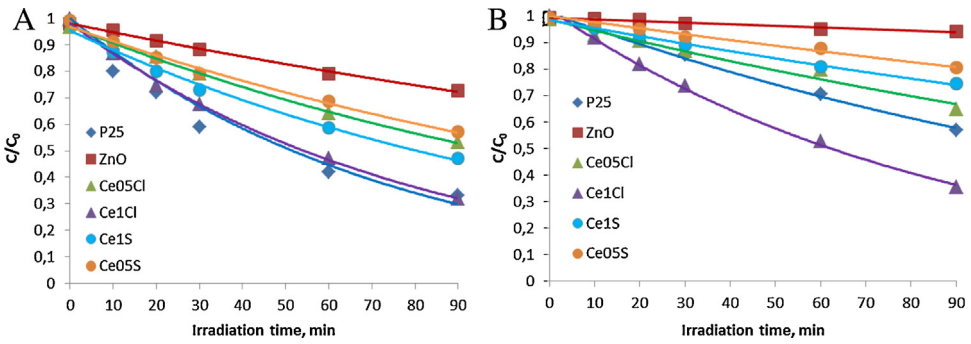

Fig. 5. ACE degradation in the presence of different catalysts under simulated UV–vis light (Panel A) and visible light (Panel B) in ultrapure water.

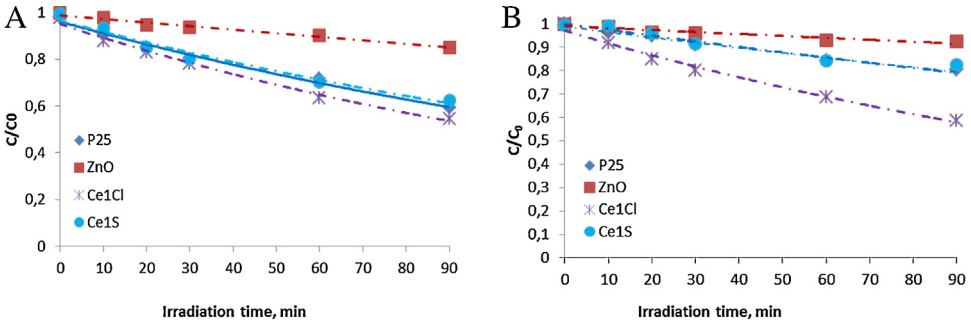

Fig. 6. ACE degradation in the presence of different catalysts under simulated solar light (Panel A) and visible light (Panel B) in river water.

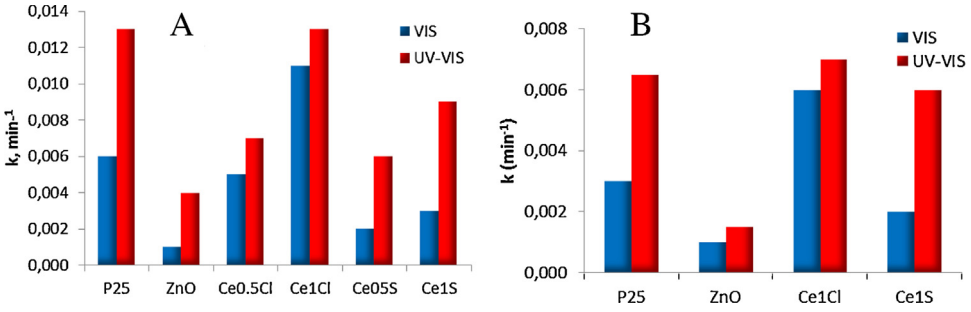

Fig. 7. Rate constants (k) of ACE decomposition by various photocatalysts under simulated solar irradiation or visible light. Panel A: ultrapure water; Panel B: river water.

not form a solid solution as in the case of CeO_2 and ZrO_2 [16], the Ce oxide acts as an "antenna" for the visible light photons, and allows some electron transfer from the discrete 4f levels to the bulk zinc oxide [11]. The nature of this electron transfer is beyond the purpose of this paper, and will be extensively studied in a forthcoming paper.

Analysing the effect of dopant salts, the increased $CeCl_3$ salt performance may lie in their different solubility, that allowed to achieve a more homogeneous dispersion of the chloride salt in the starting mixture, which led to a higher surface concentration of Ce ions in the final sample as evidenced by the XPS analysis. Secondly, a key role seems to be played by the Cerium oxidation state. By considering this aspect, XPS measures evidences that even if most of the Cerium on the material is in the form of Ce(IV), a small amount of Ce(III) is still present in the material (as shown by the XPS analysis). The presence of both Ce oxidation states could be the key to the higher activity shown by the doped samples, indeed the Ce(III)/Ce(IV) redox couple is known to be an active catalytic site for many reactions [22,23].

4. Conclusions

In this work we synthesized via an easy and cheap hydrothermal process different cerium doped zinc oxides. We used two cerium precursors for the doping ($CeCl_3$ and $Ce(SO_4)_2$) and two different percentage of dopants (0.5 and 1%). The synthesized materials have been employed in the abatement of acesulfame K, a persistent emerging contaminant, in surface water. We obtained the best performances with the sample Ce1Cl, in particular with Vis light. These new photocatalysts have been compared with the well-known TiO_2 P25. The obtained results, especially in the case of the abatement of acesulfame K in river water with the use of visible light, were surprising and unexpected. ZnO doped with cerium could represent an efficient candidate in the family of solar light photocatalysts.

Furthermore analysis concerning the transformation products and their toxicity assessment have been already planned and they will be presented in a forthcoming paper.

Acknowledgments

We acknowledge support from a Marie Curie International Research Staff Exchange Scheme Fellowship (PHOTOMAT, proposal no. 318899) within the 7th European Community Framework Programme and the project funded by MIUR, in the frame of the collaborative international consortium WATERJPI2013-MOTREM of the Water Challenges for a Changing World Joint Programming Initiative (WaterJPI) Pilot Call and Local Funding of the University of Torino call_2014_L2_126.

References

[1] Z. Sang, Y. Jiang, Y.-K. Tsoi, K.S.-Y. Leung, Evaluating the environmental impact of artificial sweeteners: a study of their distributions, photodegradation and toxicities, Water Res. 52 (2014) 260–274.
[2] S. Stolte, S. Steudte, N.H. Schebb, I. Willenberg, P. Stepnowski, Ecotoxicity of artificial sweeteners and stevioside, Environ. Int. 60 (2013) 123–127.
[3] A. Zygler, A. Wasik, J. Namiesnik, Analytical methodologies for determination of artificial sweeteners in foodstuffs, TrAC: Trends Anal. Chem. 28 (2009) 1082–1102.
[4] D. Salas, F. Borrull, N. Fontanals, R. Maria Marce, Hydrophilic interaction liquid chromatography coupled to high-resolution mass spectrometry to determine artificial sweeteners in environmental waters, Anal. Bioanal. Chem. 407 (2015) 4277–4285.
[5] R. Loos, R. Carvalho, D.C. Antonio, S. Cornero, G. Locoro, S. Tavazzi, B. Paracchini, M. Ghiani, T. Lettieri, L. Blaha, B. Jarosova, S. Voorspoels, K. Servaes, P. Haglund, J. Fick, R.H. Lindberg, D. Schwesig, B.M. Gawlik, EU-wide monitoring survey on emerging polar organic contaminants in wastewater treatment plant effluents, Water Res. 47 (2013) 6475–6487.
[6] M. Scheurer, F.R. Storck, H.-J. Brauch, F.T. Lange, Performance of conventional multi-barrier drinking water treatment plants for the removal of four artificial sweeteners, Water Res. 44 (2010) 3573–3584.
[7] Y. Liu, D.W. Blowes, L. Groza, M.J. Sabourin, C.J. Ptacek, Acesulfame-K and pharmaceuticals as co-tracers of municipal wastewater in a receiving river, Environ. Sci.: Processes Impacts 16 (2014) 2789–2795.
[8] Z. Gan, H. Sun, R. Wang, H. Hu, P. Zhang, X. Ren, Transformation of acesulfame in water under natural sunlight: joint effect of photolysis and biodegradation, Water Res. 64 (2014) 113–122.
[9] A. Fujishima, K. Hashimoto, T. Watanabe, TiO_2 Photocatalysis, Fundamentals and Applications, Bkc Inc., Tokyo, 1999.
[10] X. Chen, S.S. Mao, Titanium dioxide nanomaterials: synthesis, properties, modifications, and applications, Chem. Rev. 107 (2007) 2891–2959.
[11] S. Livraghi, M.C. Paganini, E. Giamello, A. Selloni, C. Di Valentin, G. Pacchioni, Origin of photoactivity of nitrogen-doped titanium dioxide under visible light, J. Am. Chem. Soc. 128 (2006) 15666–15671.
[12] C. Di Valentin, G. Pacchioni, Spectroscopic properties of doped and defective semiconducting oxides from hybrid density functional calculations, Acc. Chem. Res. (2014), http://dx.doi.org/10.1021/ar4002944.
[13] I.K. Konstantinou, T.A. Albanis, Photocatalytic transformation of pesticides in aqueous titanium dioxide suspensions using artificial and solar light: intermediates and degradation pathways, Appl. Catal. B 42 (2003) 319–335.
[14] N.C.S. Selvam, J.J. Vijaya, L.J. Kennedy, Effect of Ce doping on structural, optical and photocatalytic properties of ZnO nano-structures, J. Nanosci. Nanotechnol. 14 (2014) 2317–2324.
[15] K.G. Kanade, B.B. Kale, J.-O. Baeg, S.M. Lee, C.W. Lee, S.-J. Moon, H. Chang, Self-assembled aligned Cu doped ZnO nanoparticles for photocatalytic hydrogen production under visible light irradiation, Mater. Chem. Phys. 102 (2007) 98–104.
[16] C. Gionco, M.C. Paganini, E. Giamello, R. Burgess, C. Di Valentin, G. Pacchioni, Cerium-doped zirconium dioxide, a visible-light-sensitive photoactive material of third generation, J. Phys. Chem. Lett. 5 (2014) 447–451.
[17] L. Lutterotti, Total pattern fitting for the combined size-strain-stress-texture determination in thin film diffraction, Nucl. Instrum. Methods Phys. Res. Sect. B 268 (2010) 334–340.
[18] O. Bechambi, A. Touati, S. Sayadi, W. Najjar, Effect of cerium doping on the textural, structural and optical properties of zinc oxide: role of cerium and hydrogen peroxide to enhance the photocatalytic degradation of endocrine disrupting compounds, Mater. Sci. Semicond. Process. 39 (2015) 807–816.
[19] E. Beche, P. Charvin, D. Perarnau, S. Abanades, G. Flamant, Ce 3d XPS investigation of cerium oxides and mixed cerium oxide ($Ce_xTi_yO_z$), Surf. Interface Anal. 40 (2008) 264–267.
[20] A. Pfau, K.D. Schierbaum, The electronic-structure of stoichiometric and reduced CeO_2 surfaces—an XPS, UPS and HREELS study, Surf. Sci. 321 (1994) 71–80.
[21] H. Qin, W. Li, Y. Xia, T. He, Photocatalytic activity of heterostructures based on ZnO and N-doped ZnO, ACS Appl. Mater. Interfaces 3 (2011) 3152–3156.
[22] Z.A. Qiao, Z.L. Wu, S. Dai, Shape-controlled ceria-based nanostructures for catalysis applications, ChemSusChem 6 (2013) 1821–1833.
[23] Catalysis by Ceria and Related Materials, 2nd edition, World Scientific Publ. Co. Pte Ltd., Singapore, 2013.